

Performance comparison between photovoltaic and thermoradiative devices

Lin, C.; Wang, B.; Teo, K.H.; Zhang, Z.

TR2017-211 December 2017

Abstract

Photovoltaic (PV) and thermoradiative (TR) devices are power generators that use the radiative energy transfer between a hot and a cold reservoir. For PV devices, the semiconductor at the cold side (PV cell) generates electric power; for TR devices, the semiconductor at the hot side (TR cell) generates electric power. In this work, we compare the performance of the photovoltaic and thermoradiative devices, with and without the non-radiative processes. Without non-radiative processes, PV devices generally produce larger output powers than TR devices. However, when non-radiative processes become important, the TR can outperform the PV devices. This conclusion applies to both far-field and near-field based devices. A key difference in efficiency between PV and TR devices is pointed out.

Journal of Applied Physics

This work may not be copied or reproduced in whole or in part for any commercial purpose. Permission to copy in whole or in part without payment of fee is granted for nonprofit educational and research purposes provided that all such whole or partial copies include the following: a notice that such copying is by permission of Mitsubishi Electric Research Laboratories, Inc.; an acknowledgment of the authors and individual contributions to the work; and all applicable portions of the copyright notice. Copying, reproduction, or republishing for any other purpose shall require a license with payment of fee to Mitsubishi Electric Research Laboratories, Inc. All rights reserved.

Performance comparison between photovoltaic and thermoradiative devices

Chungwei Lin, Bingnan Wang, Koon Hoo Teo

Mitsubishi Electric Research Laboratories, 201 Broadway, Cambridge, MA 02139, USA

Zhuomin Zhang

George W. Woodruff School of Mechanical Engineering,

Georgia Institute of Technology, Atlanta, GA 30332, USA

(Dated: November 19, 2017)

Photovoltaic (PV) and thermoradiative (TR) devices are power generators that use the radiative energy transfer between a hot and a cold reservoir. For PV devices, the semiconductor at the cold side (PV cell) generates electric power; for TR devices, the semiconductor at the hot side (TR cell) generates electric power. In this work, we compare the performance of the photovoltaic and thermoradiative devices, with and without the non-radiative processes. Without non-radiative processes, PV devices generally produce larger output powers than TR devices. However, when non-radiative processes become important, the TR can outperform the PV devices. This conclusion applies to both far-field and near-field based devices. A key difference in efficiency between PV and TR devices is pointed out.

I. INTRODUCTION

Photovoltaic (PV) [1, 2] and thermoradiative (TR) devices [3–6] are two types of power generators that utilize the radiative energy transfer between reservoirs maintained at different temperatures. The PV devices keep the PV cell, a semiconductor, at the low temperature for power generation whereas the TR devices keep the TR cell, also a semiconductor, at the high temperature for power generation. Recently, the far-field TR performance was theoretically analyzed by Strandberg [3], and was demonstrated experimentally by Santhanam and Fan [5] with a relatively low achieved efficiency. Motivated by thermophotovoltaic (TPV), where an emitter is placed between the heat source and the cold PV cell to reshape the photon emission spectrum [7–15], placing a heat sink between the hot TR cell and the cold environment is shown to enhance the performance of TR devices [6, 16, 17]. Using the impedance matching condition derived from Coupled-Mode Theory [18–25], it is shown that the emitter and the PV cell in the near-field setup should be designed as a whole to maximize the radiative energy transfer and therefore the power output [15, 24, 26]. The same principle also applies to the TR devices, where the TR cell and the heat sink should be considered together [16, 17].

In this work, we propose a framework to compare the performances of the PV and TR devices in both the near-field and far-field configurations. The starting point is to describe the PV and TR radiative energy transfer in a unified formalism [16], which involves the transmissivity between reservoirs [24] and the generalized Planck distribution [27–29]. In this formalism, the far-field and near-field effects are encoded in the transmissivity, which can be computed using the dyadic Green function [30, 31] and the fluctuation-dissipation relation [32]. The performance will be analyzed through the current-voltage (I-V) relation, and non-radiative processes are taken into account by considering how the I-V relation is modified. The comparison between PV and TR devices is mainly based on their maximum output powers, given the same high and low reservoir temperatures T_h and T_l . The rest of the paper is organized as follows. In Section II, the performance of PV and TR devices is compared considering only the radiative process. In Section III, non-radiative processes are taken into account. The Auger process in an undoped cell is analyzed as a concrete example. In section IV, we discuss our simulation results and stress a few important points, including a key difference in efficiency between PV and TR devices. A brief conclusion is given in Section V.

II. RADIATIVE PROCESSES

A. Overview

To have a fair comparison between the PV and TR devices, the same semiconductor, characterized by the bandgap E_g , is used for PV and TR cell. The temperatures (T) of two reservoirs are fixed: for PV devices, the PV cell is kept at a low temperature $T = T_l$, whereas a heat source is kept at a high temperature $T = T_h$; for TR devices, the TR cell is kept at $T = T_h$, whereas a heat sink is fixed at $T = T_l$. In other words, the PV and TR devices, composed minimally of a semiconductor and an environment, are physically identical; the only difference is the temperature of each component. One key assumption in this setup is that, no matter how much/fast the energies are given to or taken away from a reservoir, the temperature of that reservoir does not change. The maximum output power is chosen to be the primary measure of the performance. From the practical point of view, the output power is perhaps a more important factor to consider. As an extreme example, the TR cell can approach Carnot efficiency with an infinitesimal (practically zero) output power [3, 16]. However, as the efficiency is a measure of the heat required per unit output power during the heat-to-work conversion, it becomes important if the heat dissipation rate is not fast enough to maintain the temperature (i.e., the temperature is considerably affected by the supplied heat). A more detailed discussion about efficiency will be given in Section IV. In this work, we assume the bandgap is temperature independent for model analysis; taking this effect into account is straightforward. T_h and T_l respectively represent the temperatures of the high-temperature (high-T) and low-temperature (low-T) reservoirs; we shall fix $T_l = 300$ K and allow T_h to vary.

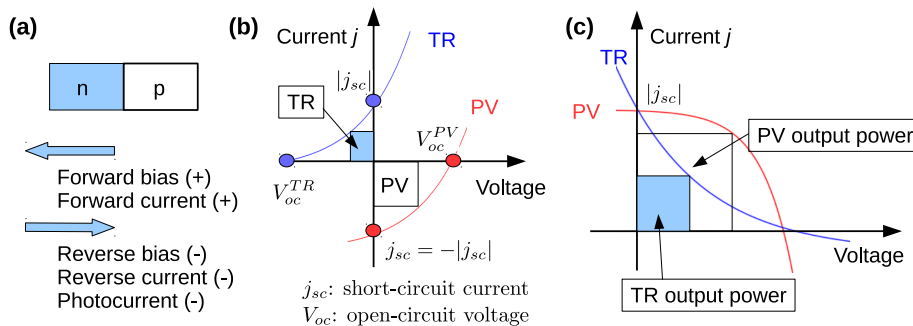


FIG. 1. (a) The sign convention of a pn-junction. The forward-bias voltage and current direction are chosen to be '+', and reverse-bias voltage and current direction to be '-'. The photo-generated current is along the reverse-bias direction. (b) Current-voltage relation for PV (red) and TR (blue) cells. The sign convention is given in (a). The areas represent the power delivered by the PV and TR devices: the larger area gives the larger output power. (c) Current-voltage relation for PV (red) cell where the sign of the current is opposite to (a), and TR (blue) cell where the sign of the voltage is opposite to (a). Using this convention, both PV and TR are described in the first quadrant with a positive output power, facilitating the discussion. Note that open-circuit voltages in (b) and (c) are not scaled but for illustration only. For a fixed temperature difference and a semiconductor of bandgap E_g , the open-circuit voltage of PV is $\lesssim E_g/|e|$; whereas that of TR is a few times the $E_g/|e|$.

B. Thermal radiative energy transfer and current-voltage relation

Let us recapitulate the formalism of the radiative energy transfer between two reservoirs [24, 26]. A reservoir is characterized by a temperature T and a voltage $V = \mu/|e|$ (e is the electron charge and μ is the photon chemical potential; μ and $|e|V$ are used interchangeably). Considering two reservoirs, labeled as 1 and 2, fixed respectively at (T_1, μ_1) and (T_2, μ_2) , the photon number flux and energy flux from 1 to 2 are given by

$$\dot{N}_{1 \rightarrow 2} = \int_0^\infty \frac{d\omega}{2\pi} \varepsilon_{12}(\omega) [\Theta(\omega; T_1, \mu_1) - \Theta(\omega; T_2, \mu_2)], \quad (1)$$

$$P_{1 \rightarrow 2} = \int_0^\infty \frac{d\omega}{2\pi} \hbar\omega \varepsilon_{12}(\omega) [\Theta(\omega; T_1, \mu_1) - \Theta(\omega; T_2, \mu_2)], \quad (2)$$

where the generalized Planck distribution [27–29] is given as $\Theta(\omega; T, \mu) = (\exp[(\hbar\omega - \mu)/T] - 1)^{-1}$, with T the temperature measured in energy, i.e., the Boltzmann constant $k_B \equiv 1$. $\varepsilon_{12}(\omega) \equiv \varepsilon(\omega)$ is the (dimensionless) transmissivity between the reservoirs 1 and 2 [24]. In the planar configurations, it is more convenient to compute the transmissivity per unit area. In this case, Eq. (1) and (2) provide the photon number flux density and the energy flux density (i.e., flux per unit area). To obtain the total photon or the energy flux, Eqs. (1) and (2) are multiplied by the area where two reservoirs exchange photons. The positive current and positive voltage are defined to be along the forward-bias direction of a pn-junction, as illustrated in Fig. 1(a). In this convention, the photocurrent is negative.

The PV devices use the low-T reservoir (PV cell) to generate the power. The photocurrent generated in the PV cell is

$$I_c = |e| \dot{N}_{T_h \rightarrow T_l} = |e| \int_0^\infty \frac{d\omega}{2\pi} \varepsilon(\omega) [\Theta(\omega; T_h, 0) - \Theta(\omega; T_l, \mu)], \quad (3)$$

The TR devices use the high-T reservoir (TR cell) to generate electric power. The photocurrent generated in the TR cell is

$$I_c = |e| \dot{N}_{T_l \rightarrow T_h} = |e| \int_0^\infty \frac{d\omega}{2\pi} \varepsilon(\omega) [\Theta(\omega; T_l, 0) - \Theta(\omega; T_h, \mu)]. \quad (4)$$

As photons of below-gap energies do not contribute to the photocurrent generation, the lower bound of integral [Eq. (3) and Eq. (4)] is taken to be the bandgap of the PV/TR cell. The Planck distribution, which decays exponentially in the large ω limit, guarantees a converged integral.

When the Planck distribution is approximated by the Boltzmann, $-I_c$ in Eq. (3) and Eq. (4) respectively reduce to

$$\begin{aligned} -I_c &\equiv j_{PV}(V) = |e| \int_0^\infty \frac{d\omega}{2\pi} \varepsilon(\omega) e^{-\hbar\omega/T_l} (e^{|e|V/T_l} - 1) + |e| \int_0^\infty \frac{d\omega}{2\pi} \varepsilon(\omega) [e^{-\hbar\omega/T_l} - e^{-\hbar\omega/T_h}], \\ -I_c &\equiv j_{TR}(V) = |e| \int_0^\infty \frac{d\omega}{2\pi} \varepsilon(\omega) e^{-\hbar\omega/T_h} (e^{|e|V/T_h} - 1) - |e| \int_0^\infty \frac{d\omega}{2\pi} \varepsilon(\omega) [e^{-\hbar\omega/T_l} - e^{-\hbar\omega/T_h}]. \end{aligned} \quad (5)$$

Defining

$$\begin{aligned} j(T) &= |e| \int_0^\infty \frac{d\omega}{2\pi} \varepsilon(\omega) e^{-\hbar\omega/T} > 0, \\ j_{sc} &= |e| \int_0^\infty \frac{d\omega}{2\pi} \varepsilon(\omega) [e^{-\hbar\omega/T_l} - e^{-\hbar\omega/T_h}] = j(T_l) - j(T_h) < 0, \end{aligned} \quad (6)$$

Eq. (5) can be expressed as

$$\begin{aligned} j_{PV}(V) &= j(T_l)(e^{|e|V/T_l} - 1) + j_{sc} = j(T_l)(e^{|e|V/T_l} - 1) - |j_{sc}| \\ j_{TR}(V) &= j(T_h)(e^{|e|V/T_h} - 1) - j_{sc} = j(T_h)(e^{|e|V/T_h} - 1) + |j_{sc}| \end{aligned} \quad (7)$$

When $T_h = T_l = T$, $j_{sc} = 0$ and $j_{PV}(V) = j_{TR}(V) = j(T)(e^{|e|V/T} - 1)$, recovering the I-V relation of a pn-junction in the dark [33]. The Boltzmann distribution well approximates the Planck, i.e., $1/(e^x - 1) \sim e^{-x}$, when the argument x is large. For $x = 1.5$, the error is about 25%; for $x = 3$, the error is about 5%. Large x corresponds to a low temperature and/or a large bandgap. Therefore, if the bandgap of the PV/TR cell is small or if the temperature is high, the Planck distribution should be used. In this work, we choose the semiconductor of a 0.2 eV bandgap, and the validity of the ‘‘Boltzmann approximation’’ is shown in Fig. 2. For $T < 800$ K, which is the temperature range of interest, the Boltzmann distribution gives the maximum error of about 5%. For the blackbody, this error becomes smaller ($< 1\%$) because the contribution of integral in large- ω region is better approximated by the Boltzmann distribution.

Eqs. (7) are illustrated in Fig. 1(b). In Fig. 1(b), the y-axis, representing the current, is $-I_c$ defined in Eqs. (3) and (4), and the x-axis is the voltage V or $\mu/|e|$. The maximum generated power is the maximum rectangular area enclosed by the I-V curves. The PV cells work in the fourth quadrant, i.e., $V > 0$ and $-I_c < 0$; the TR cells work in the second quadrant, i.e., $V < 0$ and $-I_c > 0$. For both PV and TR cells, the product of $-I_c V$ is negative, indicating power generation.

To facilitate the performance comparison between PV and TR cell, the new sign convention is adopted so that they both devices give positive I-V product in the first quadrant. For the PV cell, $\bar{j}_{PV} = -j_{PV}(V)$; for the TR cell, $\bar{j}_{TR}(V) = j_{TR}(-V)$, i.e.,

$$\begin{aligned} \bar{j}_{PV}(V) &= |j_{sc}| + j(T_l)(1 - e^{|e|V/T_l}) = j(T_h) \left[1 - \alpha(T_l, T_h) e^{|e|V/T_l} \right] \\ \bar{j}_{TR}(V) &= j(T_h)(e^{-|e|V/T_h} - 1) + |j_{sc}| = j(T_h) \left[e^{-|e|V/T_h} - \alpha(T_l, T_h) \right], \end{aligned} \quad (8)$$

with $\alpha = j(T_l)/j(T_h) < 1$. Eqs. (8) are illustrated in Fig. 1(c). In this new convention, the work done by the PV and TR cells are respectively given by $V \times \bar{j}_{PV}(V)$ and $V \times \bar{j}_{TR}(V)$, which are the rectangular areas given in Fig. 1(c). Note that $\bar{j}_{PV}(V)$ has a negative second derivative whereas $\bar{j}_{TR}(V)$ has a positive second derivative. When $V = 0$, both PV and TR have the short-circuit current $|j_{sc}| = j(T_h) - j(T_l) > 0$. The open-circuit voltages, given by $\bar{j}(V_{op}) = 0$, are $V_{op}^{PV} = T_l \log(\alpha^{-1})$ for PV cell, and $V_{op}^{TR} = T_h \log(\alpha^{-1})$ for TR cell. This device-dependent convention will be used for the rest of the paper except the first paragraph in Section III.A [Eq. (13)].

C. Blackbody and near-field resonant coupling

According to Eqs. (8), once α is known, the ratio of maximum output power between TR and PV cell is fixed. α is now computed using two forms of transmissivity. For the blackbody case, the transmissivity is given by [24]

$$\varepsilon(\omega) = \frac{1}{2\pi} \left(\frac{\omega}{c}\right)^2 \quad (9)$$

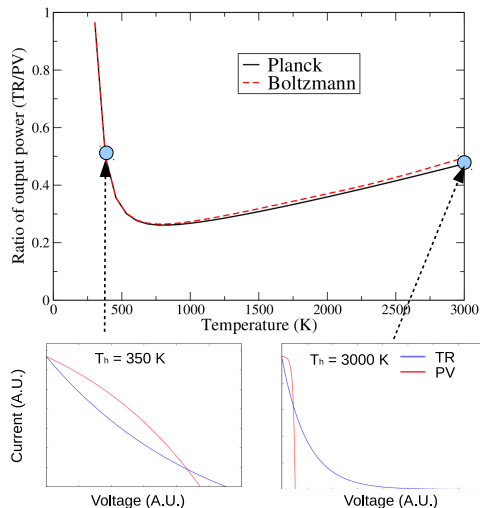


FIG. 2. The ratio of maximum output power from the TR cell and that from PV cell as a function of temperature of high-T reservoir (T_h), assuming the blackbody transmissivity. The bandgap of the PV or TR cell is $E_g = 0.2$ eV, and the low-T reservoir is fixed $T_l = 300$ K. When T_h is smaller than the corresponding E_g , using the Boltzmann distribution (red dashed curve) instead of the exact Planck (black solid curve) gives a very good approximation. For a wide temperature range ($T_h \lesssim 6000$ K in this example), the PV has a larger output power. This ratio is at minimum when $T_h \approx 730$ K. Below $T_h = 1500$ K ($\lesssim E_g$), using Boltzmann distribution gives almost identical results to those using the exact Planck distribution. (Bottom) The representative I-V curves at different T_h . The blue/red curve corresponds to TR/PV cell. The units are arbitrary, but the relative amplitudes between PV and TR, for both current and voltage, are preserved. When $T_h \gtrsim T_l$ ($T_h = 350$ K, left one), both PV and TR have similar open-circuit voltage, and their I-V curves are close to straight lines. PV has slightly larger output power because its negative second derivative of I-V curves. When $T_h \gg T_l$ ($T_h = 3000$ K, right one), the TR has a much larger open-circuit voltage, allowing TR cell to have a comparable output power to PV cell.

Using Eq. (9), α has an analytical expression as

$$\alpha_{BB}(E_g, T_l, T_h) = \left[\frac{T_l}{T_h} \right]^3 \times \frac{e^{-E_g/T_l}}{e^{-E_g/T_h}} \times \frac{(E_g/T_l)^2 + 2(E_g/T_l) + 2}{(E_g/T_h)^2 + 2(E_g/T_h) + 2}. \quad (10)$$

The subscript 'BB' denotes the blackbody limit. In the case where the photon exchanges are dominated by the near-field resonant coupling, the transmissivity can be approximated by a δ -function [16], i.e.,

$$\varepsilon(\hbar\omega) = C\delta(\hbar\omega - \hbar\omega_0), \quad (11)$$

with $\hbar\omega_0 > E_g$ and C some constant. For convenience, $\hbar\omega_0 = E_g$ is assumed. In this case, α has a simpler analytical expression as

$$\alpha_{NF}(E_g, T_l, T_h) = \frac{e^{-E_g/T_l}}{e^{-E_g/T_h}} \quad (12)$$

The subscript 'NF' denotes the near-field coupling.

In both Eq. (10) and Eq. (12), when $T_h \gg T_l$, the exponential factor $e^{-E_g/T_l}/e^{-E_g/T_h}$ dominates and α is a very small number; when $T_h \gtrsim T_l$, α is slightly smaller than one. As α_{BB} and α_{NF} have very similar behavior, their respective comparison of PV and TR performances is also similar. Fig. 2 gives the ratio of maximum output power from the TR cell and that from PV cell as a function of temperature of high-T reservoir (T_h), assuming the blackbody transmissivity [Eq. (9)] with $E_g = 0.2$ eV, which is roughly the bandgap of InSb [34]. The low-T reservoir is fixed $T_l = 300$ K. For the whole practically feasible temperature range, the PV is found to produce a larger output power. At the impractically high temperature (e.g. $T_h = 8000$ K, not shown), the TR can produce a larger output power due to its large open-circuit voltage. When $T_h \lesssim 1500$ K, the results of using the Boltzmann distribution and the exact Planck distribution are very similar, justifying the validity of Eqs. (5). We also mention that the δ -function transmissivity [Eq. (11)] gives a very similar behavior [see Fig. 4(a)].

D. Critical parameter and temperature regime of interest

Based on the preceding discussion, the most critical parameter to determine the relative performance of PV and TR cells is α defined in Eqs. (8). Due to the similar behavior of α computed from Eq. (10) and Eq. (12), the conclusion that PV outperforms TR holds for both far-field and near-field based devices, as long as only the radiative process is considered. However, one bears in mind that the near-field setup can give a much larger output power, for both PV and TR devices. In terms of Eqs. (8), $j(T_h)$ affects the actual output power of PV and TR cell, but plays no role on the *ratio* of PV and TR output power.

For realistic applications, the temperature of TR cell cannot be too high. The temperature of 4000 K is so high that the existence or the stability of TR cells is doubtful. Also, increasing the temperature generally increases the resistivity of the semiconductor, which is detrimental to the power generation. To be relevant to the practical interest, only the temperature range $T_h < 800$ K (roughly the melting point of InSb) is considered for the remaining of our discussion.

III. NON-RADIATIVE PROCESSES

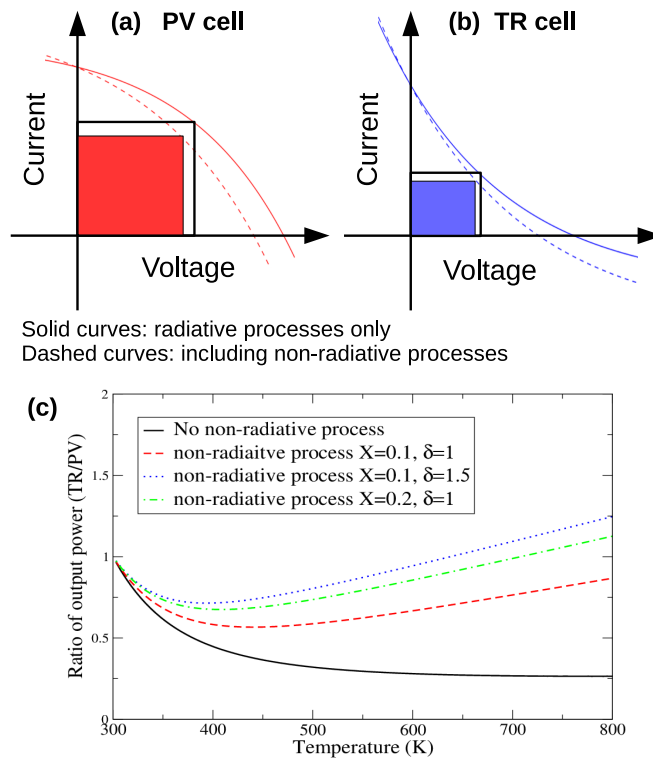


FIG. 3. (a) The I-V curve of PV cell, with (dashed curve) and without (solid curve) the non-radiative processes. (b) The I-V curve of TR cell, with (dashed curve) and without (solid curve) the non-radiative processes. In both cases, including non-radiative processes reduces the open-circuit voltage and the output power (indicated by the area). (c) The ratio of maximum output power from the TR cell and that from PV cell, with (dashed curve) and without (solid curve) the non-radiative processes. The non-radiative calculation is done using $X_1 = 0.1$, $\delta_1 = 1$ (red dashed curve), $X_1 = 0.1$, $\delta_1 = 1.5$ (blue dotted curve), and $X_1 = 0.2$, $\delta_1 = 1$ (green, dash-dot curve). With non-radiative processes, the TR output power can become larger than the PV output power. All other parameters are same as those in Fig. 2.

A. Overview and the main picture

The inclusions of non-radiative processes affect the I-V curve. A non-radiative process provides one channel for electrons and holes to recombine, and each has its own I-V characteristic given by [35, 36]

$$j_i^{(NR)}(V) = j(T)X_i(T)(e^{\delta_i|e|V/T} - 1), \quad (13)$$

with the sign convention defined in Fig. 1(a) and (b). Here i labels the non-radiative process, T is the cell temperature, X_i is a dimensionless (but temperature-dependent) parameter that characterizes the relative strength between the radiative and the non-radiative process, and δ_i specifies the voltage dependence. Short derivations of Eq. (13) for impurity and Auger processes will be given in the Appendices. The basic physics picture is that, once the electron and hole concentrations are different from their equilibrium values, a non-radiative process also produces a current (in addition to the current generated by the radiative process). The exponential voltage dependence reflects the dependence on electron and hole concentrations, and the -1 in the parenthesis ensures that there is no current at zero voltage. The total I-V curve is the sum of Eqs. (7) and Eq. (13).

Switching back to the sign convention given in Fig. 1(c), and adding Eq. (13) to Eqs. (8), the total I-V curves for both PV and TR cell are

$$\begin{aligned} \bar{j}_{PV}(V) &= j(T_l) \left[1 - \alpha(T_l, T_h)e^{|e|V/T_l} + \sum_i X_i(1 - e^{\delta_i|e|V/T_l}) \right] \\ \bar{j}_{TR}(V) &= j(T_h) \left[e^{-|e|V/T_h} - \alpha(T_l, T_h) - \sum_i X_i(1 - e^{-\delta_i|e|V/T_h}) \right], \end{aligned} \quad (14)$$

Here i 's denote the non-radiative processes. Fig. 3(a) and (b) respectively compare the PV and TR I-V curves with and without non-radiative processes. Including non-radiative processes reduces the open-circuit voltages and the maximum output power, because some of photon-generated electron-hole pairs are recombined through those processes.

Eq. (14) shows that $\bar{j}_{PV}(V)$ has a negative second derivative (with respect to V) whereas $\bar{j}_{TR}(V)$ positive [see Fig. 3(a) and (b)]. Therefore, as the voltage V increases, the non-radiative process suppresses the current in PV cell faster than in TR cell, which leads to a larger output power reduction in the PV cell than the TR. This general behavior can be seen in Fig. 3(c), which shows the ratio of maximum output power from the TR cell and that from PV cell, with the non-radiative processes specified by $(X_1, \delta_1) = (0.1, 1)$, $(0.1, 1.5)$, and $(0.2, 1)$. For now the temperature dependence on X_1 is ignored. All other parameters are same as those in Fig. 2. The inclusion of non-radiative processes indeed favors the TR devices. When they are strong, the TR output power can be larger than the PV output power. Eqs. (14) provide the general framework on how to take the non-radiative processes into account, and the next step is to estimate the parameters for the performance comparison between PV and TR cells.

B. Auger process in the undoped cell: output power

To more quantitatively model the non-radiative processes, the geometry of the PV or TR cell has to be specified. We take the cell to be a slab, with a volume $V_{cell} = A_i \times L_z$. Here A_i is the ‘‘photon-exchange’’ area through which photons are absorbed or emitted, and L_z is thickness of the cell. The other side of the slab is covered by a reflective metal. A_i multiplied by Eqs. (7) or Eqs. (8) give the *total* photocurrent, whereas V_{cell} multiplied by Eq. (A6) [37], Eq. (A8) [36], or Eq. (A10) [35] gives the total current generated by the non-radiative process. To determine the X_i of Eq. (13), only the thickness L_z is needed. For a general geometry, L_z is replaced by the cell volume divided by the photon-exchange area. We also note that when non-radiative processes are considered, $j(T_h)$ affects the output power ratio between PV and TR cell; this is not the case when considering only the radiative process [see Section II.C and II.D].

The non-radiative Auger process for an undoped semiconductor is now considered. From Appendix [see Eq. (A8)], one gets

$$j(T_h)X_{Auger} = |e|(A_e + A_h)n_i^3 \times L_z, \quad (15)$$

To be concrete, we consider InSb, with a bandgap of ~ 0.2 eV, an intrinsic carrier concentration of $\sim 2 \cdot 10^{16}$ cm^{-3} and the Auger coefficient of $(A_e + A_h) \sim 5 \cdot 10^{-26}$ $\text{cm}^{-6} \text{s}^{-1}$ [38]. Taking $L_z = 250$ nm, one gets $|e|(A_e + A_h)n_i^3 L_z \sim 1.6$ A cm^{-2} . For simplicity this value is assumed to be temperature independent over the temperature range of interest [39].

$j(T_h)$ and X for both blackbody and near-field transmissivities are now computed. For the far-field blackbody limit, Eq. (9) is used to obtain

$$j_{BB}(T_h) \sim \left(\frac{T_h}{\text{eV}}\right)^3 \left[\left(\frac{E_g}{T_h}\right)^2 + 2\frac{E_g}{T_h} + 2 \right] e^{-E_g/T_h} \cdot 1.6 \cdot 10^4 \text{ A cm}^{-2},$$

$$X_{Auger, BB} \sim \left\{ \left(\frac{T_h}{\text{eV}}\right)^3 \left[\left(\frac{E_g}{T_h}\right)^2 + 2\frac{E_g}{T_h} + 2 \right] \right\}^{-1} e^{+E_g/T_h} \cdot 10^{-4}.$$
(16)

In these expressions, T_h is understood as $k_B T$ and has the dimension of energy. For the near-field device, C in Eq. (11) is taken to be $4.13 \cdot 10^8$ eV cm^{-2} , a value estimated from Ref. [16]. The near-field $j(T_h)$ and X are accordingly

$$j_{NF}(T_h) = e^{-E_g/T_h} 1.6 \cdot 10^4 \text{ A cm}^{-2},$$

$$X_{Auger, NF} \sim e^{+E_g/T_h} \cdot 10^{-4}.$$
(17)

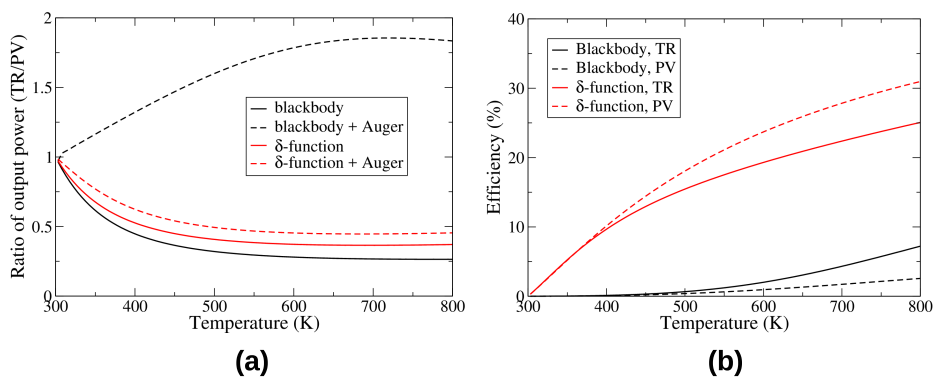


FIG. 4. (a) The ratio of maximum output power from the TR cell and from PV cell, with (dashed curves) and without (solid curves) the non-radiative Auger process. For the blackbody transmissivity (black curves), the Auger generated current is large compared to the photocurrent generated by the blackbody transmissivity, the TR device is favored for the whole the temperature range. For the near-field δ -function transmissivity (red curves), the Auger generated current is small compared to the photocurrent generated by the δ -function transmissivity, the PV device is favored for the whole the temperature range. (b) The efficiency of PV and TR devices with the Auger process [see two dashed curves in (a)]. Two black curves give the TR (solid black) and PV (dashed black) efficiencies for blackbody, corresponding to the black dashed curve in (a); the TR has a higher efficiency. Two red curves give the TR (solid red) and PV (dashed red) efficiencies for near-field, corresponding to the red dashed curve in (a); the PV has a higher efficiency.

Fig. 4(a) shows the ratio of maximum output power from the TR cell and from PV cell, with and without the non-radiative Auger process in the undoped PV and TR cells. For the blackbody transmissivity, the Auger generated current is large compared to the photocurrent generated by the blackbody transmissivity (large X), the TR device is favored for the whole the temperature range. For the near-field δ -function transmissivity, the Auger generated current is small compared to the photocurrent generated by the δ -function transmissivity (small X), the PV device is favored for the whole the temperature range. While only the intrinsic Auger process is explicitly considered here, our analysis can be straightforwardly applied to any non-radiative processes.

IV. DISCUSSION

In this section, we discuss our simulation results, and comment on a few important points which are not included in this work. First, our results show that including the non-radiative process generally favors the TR cell. Non-

radiative processes always suppress the output power, but they reduce TR output power less than PV output power. Due to the small bandgap of the InSb cell, the Auger generated current is large (originated from large n_i). When the photocurrent is small, such as the case of the blackbody transmissivity, the TR outperforms the PV device. In the other limit where the photocurrent is large, such as the case of the near-field δ -function transmissivity, the PV outperforms the TR device. Somewhere between these two limits, there exists a parameter regime where PV and TR perform comparably. Second, one notes that the cell thickness L_z has two opposite effects. On the one hand, large L_z increases the number of absorbed photons and thus the output power. On the other hand, large L_z increases the current generated by all non-radiative processes, reducing the output power. Generally, the L_z is chosen to be a few times larger than the inverse of the absorption coefficient.

We now comment on the efficiency of PV and TR devices. The efficiency η of a power generation device is given by the ratio between the output power P_{load} and the absorbed heat flux. For PV and TR devices, they are

$$\eta_{PV} = \frac{P_{load}}{\dot{E}_{abs} - \dot{E}_{rad}} \quad (18)$$

$$\eta_{TR} = \frac{P_{load}}{P_{load} + \dot{E}_{rad} - \dot{E}_{abs}}. \quad (19)$$

Here, \dot{E}_{rad} and \dot{E}_{abs} are respectively the energy flux radiated from and absorbed by the cell, and their difference $\dot{E}_{rad} - \dot{E}_{abs}$ (positive for TR; negative for PV) is the net emission power from the cell, which can be computed using Eq. (2). A key difference between η_{TR} and η_{PV} is that the output power P_{load} appears in both numerator and denominator of η_{TR} , whereas only in numerator of η_{PV} . Consequently, the non-radiative reduction of P_{load} suppresses the PV efficiency η_{PV} more than the TR efficiency η_{TR} . This difference originates from the fact that in PV cells, non-radiative recombinations are associated with a loss of energy, whereas in TR cells, non-radiative generations of electron-hole pairs simply reduce the open-circuit voltage, but the energy is not lost but still present in the cell. When comparing the PV and TR efficiency at the maximum-power point, the larger output power usually corresponds to a higher efficiency. These results are illustrated in Fig. 4(b). Note that the maximum TR efficiency can be high (close to Carnot efficiency), but with a very small output power [3]. This case is not of our interest and is not considered here.

Finally, we remark on the free-carrier effect, which is not taken into account but is important in the high-temperature, small bandgap devices. The free-carrier effect accounts for photon-induced intra-band transitions [40]. Due to the small photon momentum, the intra-band photon absorption and emission are always accompanied with other scatterings such as phonons or impurities. A standard approach to include this effect is to add a small Drude term to the dielectric function of the PV/TR cell (semiconductor) [15, 41], whose amplitude and decay rate are temperature-dependent. As the free-carrier effect introduces an additional loss mechanism, it reduces the output powers for PV/TR devices using the far-field setup. For the near-field setup, however, the loss can sometimes enhance the radiative energy transfer [15, 16, 24], and a more detailed model is needed to quantify its effect.

V. CONCLUSION

To conclude, the main question we address and answer is: from the fundamental physics point of view, for a given semiconductor, a high temperature T_h and a low temperature T_l , how to compare the PV with the TR as a power generator? The maximum electric output power is chosen as the main metric for performance comparison. The radiative energy transfer between the PV/TR cell and the environment is described by the transmissivity. The PV and TR current-voltage relations, including both radiative and non-radiative processes, are then used to obtain the maximum output power. The formalism applies to both far-field and near-field based devices. When only the radiative process is considered, a dimensionless parameter α is identified that fully characterizes the relative performance of PV and TR devices. Under this condition, PV devices produce larger output powers than TR devices in the feasible (low) temperature range; the TR can outperform the PV at impractically high temperature. When the non-radiative processes are included, an additional dimensionless parameter X_i for each non-radiative process is needed. Non-radiative processes generally favor the TR performance, in the sense that they suppress the PV output power and efficiency more significantly than the TR. When non-radiative processes become important, the TR can outperform the PV devices in the temperature range of interest. The conclusion applies to both far-field and near-field based devices. Our analysis provides a guide on how to choose between PV and TR devices in an application.

ACKNOWLEDGEMENT

We thank an anonymous reviewer for pointing out the key difference in efficiency between TR and PV devices. Z.M.Z. would like to thank the support from the U.S. Department of Energy, Office of Science, Basic Energy Sciences (Grant No. DE-SC0018369).

Appendix A: Impurity and Auger processes

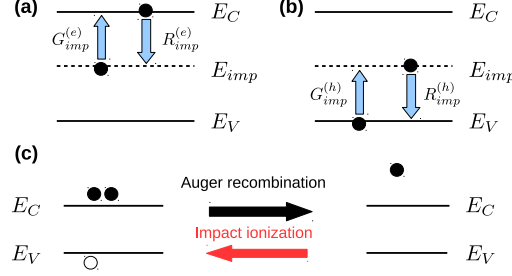


FIG. 5. (a) Electron generation and recombination via impurities. The electron generation rate is proportional to the impurity level occupation; the electron recombination rate is proportional to the product of electron concentration and the probability where an impurity is unoccupied. (b) Hole generation and recombination via impurities. The hole generation rate is proportional to the probability where the impurity level is empty; the hole recombination rate is proportional to the product of hole concentration and the probability where an impurity is occupied. The arrow indicates the transition of *electron* (filled circle). (c) The impact ionization and Auger recombination. The impact ionization generates an e-h pair from a high-energy electron. For the Auger recombination, the photon generated by recombining an e-h pair is transferred to a low-energy electron. These two processes are reverse to each other. E_V , E_C , E_{imp} are respectively the energies of valance band top, conduction band bottom, and the impurity level.

In the Appendix we provide short derivations on the electron-hole (e-h) generation/recombination via impurities and Auger processes. Using the sign convention defined in Fig. 1(a), the e-h generation provides the “negative” current, whereas the e-h recombination the “positive” current. The goal is to obtain the current caused by these processes under an external voltage.

1. e-h recombination and generation due to impurities

The impurity mediated combination is typically referred to as the Shockley-Read-Hall recombination [37]. The rate equation for the electron concentration is [Fig.5(a)]

$$\frac{\partial n_e}{\partial t} = G_{imp}^{(e)} - R_{imp}^{(e)} = C_e n_{imp} f(E_{imp}) - \alpha_e n_e n_{imp} (1 - f(E_{imp})) \quad (A1)$$

The electron generation rate is proportional to the impurity level occupation; the electron recombination rate is proportional to the product of electron concentration and the probability where an impurity is unoccupied. Thermal equilibrium ($\frac{\partial n_e}{\partial t} = 0$ and $f(E)$ is the Fermi distribution) implies $C_e = \alpha_e n_{e,0} e^{(E_{imp} - E_F)/T} \equiv \alpha_e n_1$, and Eq. (A1) becomes $\frac{\partial n_e}{\partial t} = \alpha_e n_{imp} [(n_e + n_1) f(E_{imp}) - n_e]$. Similarly, the rate equation for the hole concentration is [Fig.5(b)]

$$\frac{\partial n_h}{\partial t} = G_{imp}^{(h)} - R_{imp}^{(h)} = C_h n_{imp} (1 - f(E_{imp})) - \alpha_h n_h n_{imp} f(E_{imp}) \quad (A2)$$

The hole generation rate is proportional to the probability where the impurity level is empty; the hole recombination rate is proportional to the product of hole concentration and the probability where an impurity is occupied. Thermal equilibrium implies $C_h = \alpha_h n_{h,0} e^{-(E_{imp} - E_F)/T} \equiv \alpha_h h_1$ and Eq. (A2) becomes $\frac{\partial n_h}{\partial t} = \alpha_h n_{imp} [-(n_h + h_1) f(E_{imp}) + h_1]$. The net electron generating rate is thus

$$\frac{\partial n_e}{\partial t} = \frac{\partial n_h}{\partial t} = -\frac{\alpha_e \alpha_h n_{imp} (n_e n_h - n_i^2)}{\alpha_e (n_e + n_1) + \alpha_h (n_h + h_1)}, \quad (A3)$$

where $n_1 h_1 = n_i^2$, with n_i the electron (and hole) concentration of the intrinsic undoped semiconductor is used. The net generating rate is only non-zero when $n_e n_h - n_i^2 \neq 0$; it always tends to recover the original e-h pair density, i.e., electrons and holes are generated when $n_e n_h < n_i^2$; annihilated when $n_e n_h > n_i^2$.

We would like to express Eq. (A3) in terms of quasi Fermi energies, E_{FC} and E_{FV} . In order to do this, it is convenient to use the *undoped* Fermi energy E_i as the reference energy, and the undoped electron concentration $n_i = N_c e^{-(E_C - E_i)/T} = P_v e^{-(E_i - E_V)/T}$ as the reference concentration. With some algebra, we get

$$\begin{aligned} n_e &= n_i e^{-(E_i - E_{FC})/T}, n_h = n_i e^{-(E_{FV} - E_i)/T}, \\ n_1 &= n_i e^{-(E_i - E_{imp})/T}, h_1 = n_i e^{-(E_{imp} - E_i)/T} \end{aligned} \quad (\text{A4})$$

Inserting Eqs. (A4) into Eq. (A3), we get

$$\frac{\partial n_e}{\partial t} = \frac{\partial n_h}{\partial t} = -\frac{n_i [e^{(E_{FC} - E_{FV})/T} - 1]}{[e^{(E_{FC} - E_i)/T} + e^{(E_{imp} - E_i)/T}] / (\alpha_h n_{imp}) + \tau_{e,min} [e^{(E_i - E_{FV})/T} + e^{(E_i - E_{imp})/T}] / (\alpha_e n_{imp})}, \quad (\text{A5})$$

To allow for an analytical expression, we assume $E_i = E_{imp}$ and the electron-hole symmetry, i.e. $\alpha_e = \alpha_h \equiv \alpha$ and $E_{FC} - E_i = E_i - E_{FV} = |e|V/2$ to get

$$G_{imp} - R_{imp} = -n_{imp} \alpha n_i \frac{e^{(E_{FC} - E_{FV})/T} - 1}{e^{(E_{FC} - E_i)/T} + e^{(E_i - E_{FV})/T} + 2} = -\frac{n_{imp} \alpha n_i}{2} \left[\exp \frac{|e|V}{2T} - 1 \right]. \quad (\text{A6})$$

Here $E_{FC} - E_{FV} = |e|V$ is used. Eq. (A6) gives the $(e^{|e|V/(2T)} - 1)$ voltage dependence of the current [2, 37].

2. Auger recombination and impact ionization

Here we describe the e-h generation via the impact ionization and the e-h recombination via the Auger recombination [35, 36]. As illustrated in Fig. 5(c), the impact ionization generates a e-h pair from a high-energy electron. For the Auger recombination, the photon generated by recombining a e-h pair is transferred to a low-energy electron. The Auger recombination rate is

$$\begin{aligned} R_{Aug} &= R_{Aug,e} + R_{Aug,h} = A_e n_e^2 n_h + A_h n_e n_h^2 = n_e n_h (A_e n_e + A_h n_h) \\ &\rightarrow n_i^2 e^{(E_{FC} - E_{FV})/T} \left[A_e n_i e^{(E_{FC} - E_i)/T} + A_h n_i e^{(E_i - E_{FV})/T} \right] \\ &\rightarrow n_i^2 e^{|e|V/T} \left[A_e n_i e^{|e|V/(2T)} + A_h n_i e^{|e|V/(2T)} \right] = (A_e + A_h) n_i^3 \exp \frac{3|e|V}{2T}. \end{aligned} \quad (\text{A7})$$

A_e and A_h are the Auger coefficients for electrons and holes. The second line is still exact, but uses the parametrization of Eqs. (A4). The last line assumes $E_{FC} - E_i = E_i - E_{FV} = |e|V/2$ as the impurity case. The corresponding impact ionization rate can be obtained from the equilibrium situation: $G_{Aug} = n_{e,0} n_{h,0} (A_e n_{e,0} + A_h n_{h,0}) \rightarrow n_i^3 (A_e + A_h)$. The last expression assumes the intrinsic semiconductor $n_{e,0} = n_{h,0} = n_i$. Combining all the approximations, we have

$$\frac{\partial n_e}{\partial t} = \frac{\partial n_h}{\partial t} = G_{Aug} - R_{Aug} = -(A_e + A_h) n_i^3 \left[\exp \frac{3|e|V}{2T} - 1 \right]. \quad (\text{A8})$$

In the heavily n-doped limit, n_e concentration is fixed by the doping concentration $n_e \approx n_{imp,e} \gg n_h$. In this case, Auger recombination rate is

$$\begin{aligned} R_{Aug} &= R_{Aug,e} + R_{Aug,h} = A_e n_e^2 n_h + A_h n_e n_h^2 = n_e n_h (A_e n_e + A_h n_h) \approx n_e n_h (A_e n_{imp,e}) \\ &\rightarrow n_i^2 e^{(E_{FC} - E_{FV})/T} [A_e n_{imp,e}] = A_e n_{imp,e} n_i^2 e^{|e|V/T} \end{aligned} \quad (\text{A9})$$

Combining the corresponding impact ionization rate, we have

$$\frac{\partial n_e}{\partial t} = \frac{\partial n_h}{\partial t} = G_{Aug} - R_{Aug} = -A_e n_{imp,e} n_i^2 \left[\exp \frac{|e|V}{T} - 1 \right] \quad (\text{A10})$$

in the heavily n-doping limit. A similar expression can be obtained for the heavily p-doping case. Therefore, the Auger process gives a $(e^{3|e|V/(2T)} - 1)$ voltage dependence in the intrinsic limit; a current of $(e^{|e|V/T} - 1)$ voltage dependence in the heavily doped limit.

-
- [1] William Shockley and Hans J. Queisser, “Detailed balance limit of efficiency of p-n junction solar cells,” *Journal of Applied Physics* **32**, 510–519 (1961).
- [2] Peter Würfel, *Physics of Solar Cells* (Wiley-vch, 2005).
- [3] Rune Strandberg, “Theoretical efficiency limits for thermoradiative energy conversion,” *Journal of Applied Physics* **117**, 055105 (2015), <http://dx.doi.org/10.1063/1.4907392>.
- [4] Rune Strandberg, “Heat to electricity conversion by cold carrier emissive energy harvesters,” *Journal of Applied Physics* **118**, 215102 (2015), <http://dx.doi.org/10.1063/1.4936614>.
- [5] Parthiban Santhanam and Shanhui Fan, “Thermal-to-electrical energy conversion by diodes under negative illumination,” *Phys. Rev. B* **93**, 161410 (2016).
- [6] Wei-Chun Hsu, Jonathan K. Tong, Bolin Liao, Yi Huang, Svetlana V. Boriskina, and Gang Chen, “Entropic and near-field improvements of thermoradiative cells,” *Scientific Reports* **6**, 34837 (2016/10/13/online).
- [7] P.A. Davies and A. Luque, “Solar thermophotovoltaics: brief review and a new look,” *Solar Energy Materials and Solar Cells* **33**, 11 – 22 (1994).
- [8] Nils-Peter Harder and Peter Würfel, “Theoretical limits of thermophotovoltaic solar energy conversion,” *Semiconductor Science and Technology* **18**, S151 (2003).
- [9] Peter Bermel, Michael Ghebrebrhan, Walker Chan, Yi Xiang Yeng, Mohammad Araghchini, Rafif Hamam, Christopher H. Marton, Klavs F. Jensen, Marin Soljačić, John D. Joannopoulos, Steven G. Johnson, and Ivan Celanovic, “Design and global optimization of high-efficiency thermophotovoltaic systems,” *Opt. Express* **18**, A314–A334 (2010).
- [10] M. Francoeur, R. Vaillon, and M. P. Meng, “Thermal impacts on the performance of nanoscale-gap thermophotovoltaic power generators,” *IEEE Transactions on Energy Conversion* **26**, 686–698 (2011).
- [11] Yi Xiang Yeng, Walker R. Chan, Veronika Rinnerbauer, John D. Joannopoulos, Marin Soljačić, and Ivan Celanovic, “Performance analysis of experimentally viable photonic crystal enhanced thermophotovoltaic systems,” *Opt. Express* **21**, A1035–A1051 (2013).
- [12] Riccardo Messina and Philippe Ben-Abdallah, “Graphene-based photovoltaic cells for near-field thermal energy conversion,” *Scientific Reports* **3**, 1383 (2013).
- [13] Andrej Lenert, David M. Bierman, Youngsuk Nam, Walker R. Chan, Ivan Celanović, Marin Soljagic, and Evelyn N. Wang, “A nanophotonic solar thermophotovoltaic device,” *Nat Nano* **9**, 126–130 (2014).
- [14] David M. Bierman, Andrej Lenert, Walker R. Chan, Bikram Bhatia, Ivan Celanović, Marin Soljagic, and Evelyn N. Wang, “Enhanced photovoltaic energy conversion using thermally based spectral shaping,” *Nature Energy* **1**, 16068 (2016).
- [15] Aristeidis Karalis and J. D. Joannopoulos, “Squeezing near-field thermal emission for ultra-efficient high-power thermophotovoltaic conversion,” *Scientific Reports* **6**, 141108 (2016), [10.1038/srep28472](https://doi.org/10.1038/srep28472).
- [16] Chungwei Lin, Bingnan Wang, Koon Hoo Teo, and Zhuomin Zhang, “Near-field enhancement of thermoradiative devices,” *Journal of Applied Physics* **122**, 143102 (2017).
- [17] Bingnan Wang, Chungwei Lin, Koon Hoo Teo, and Zhuomin Zhang, “Thermoradiative device enhanced by near-field coupled structures,” *Journal of Quantitative Spectroscopy and Radiative Transfer* **196**, 10–16 (2017).
- [18] H. A. Haus and W. Huang, “Coupled-mode theory,” *Proceedings of the IEEE* **79**, 1505–1518 (1991).
- [19] Allan W. Snyder, “Coupled-mode theory for optical fibers,” *J. Opt. Soc. Am.* **62**, 1267–1277 (1972).
- [20] Wei-Ping Huang, “Coupled-mode theory for optical waveguides: an overview,” *J. Opt. Soc. Am. A* **11**, 963–983 (1994).
- [21] Shanhui Fan, Wonjoo Suh, and J. D. Joannopoulos, “Temporal coupled-mode theory for the fano resonance in optical resonators,” *J. Opt. Soc. Am. A* **20**, 569–572 (2003).
- [22] Hamidreza Chalabi, Erez Hasman, and Mark L. Brongersma, “An ab-initio coupled mode theory for near field radiative thermal transfer,” *Opt. Express* **22**, 30032–30046 (2014).
- [23] Linxiao Zhu, Sunil Sandhu, Clayton Otey, Shanhui Fan, Michael B. Sinclair, and Ting Shan Luk, “Temporal coupled mode theory for thermal emission from a single thermal emitter supporting either a single mode or an orthogonal set of modes,” *Applied Physics Letters* **102**, 103104 (2013), <http://dx.doi.org/10.1063/1.4794981>.
- [24] Aristeidis Karalis and J. D. Joannopoulos, “Temporal coupled-mode theory model for resonant near-field thermophotovoltaics,” *Applied Physics Letters* **107**, 141108 (2015), <http://dx.doi.org/10.1063/1.4932520>.
- [25] Chungwei Lin, Bingnan Wang, and Koon Hoo Teo, “Application of coupled mode theory on radiative heat transfer between layered Lorentz materials,” *Journal of Applied Physics* **121**, 183101 (2017).
- [26] Chungwei Lin, Bingnan Wang, Koon Hoo Teo, and Prabhakar Bandaru, “Application of impedance matching for enhanced transmitted power in a thermophotovoltaic system,” *Phys. Rev. Applied* **7**, 034003 (2017).

- [27] P Würfel, “The chemical potential of radiation,” *Journal of Physics C: Solid State Physics* **15**, 3967 (1982).
- [28] Berndt Feuerbacher and Peter Würfel, “Verification of a generalised Planck law by investigation of the emission from gaas luminescent diodes,” *Journal of Physics: Condensed Matter* **2**, 3803 (1990).
- [29] P. Würfel, S. Finkbeiner, and E. Daub, “Generalized Planck’s radiation law for luminescence via indirect transitions,” *Applied Physics A* **60**, 67–70 (1995).
- [30] D. Polder and M. Van Hove, “Theory of radiative heat transfer between closely spaced bodies,” *Phys. Rev. B* **4**, 3303–3314 (1971).
- [31] Karl Joulain, Jean-Philippe Mulet, Franois Marquier, Rmi Carminati, and Jean-Jacques Greffet, “Surface electromagnetic waves thermally excited: Radiative heat transfer, coherence properties and casimir forces revisited in the near field,” *Surface Science Reports* **57**, 59 – 112 (2005).
- [32] Herbert B. Callen and Theodore A. Welton, “Irreversibility and generalized noise,” *Phys. Rev.* **83**, 34–40 (1951).
- [33] Neil W. Ashcroft and N. David Mermin, *Solid State Physics* (Saunders College Publishing, 1976).
- [34] Sadao Adachi, “Optical dispersion relations for GaP, GaAs, GaSb, InP, InAs, and InSb, $\text{Al}_x\text{Ga}_{1-x}\text{As}$, and $\text{In}_{1-x}\text{Ga}_x\text{As}_y\text{P}_{1-y}$,” *Journal of Applied Physics* **66**, 6030–6040 (1989), <http://dx.doi.org/10.1063/1.343580>.
- [35] Martin A. Green, “Limits on the open-circuit voltage and efficiency of silicon solar cells imposed by intrinsic auger processes,” *IEEE Transactions on Electron Devices* **31**, 671–678 (1984).
- [36] Uli Würfel, Dieter Neher, Annika Spies, and Steve Albrecht, “Impact of charge transport on current-voltage characteristics and power-conversion efficiency of organic solar cells,” *Nature Communications* **6**, 6951 (2015).
- [37] W. Shockley and W. T. Read, “Statistics of the recombinations of holes and electrons,” *Phys. Rev.* **87**, 835–842 (1952).
- [38] S Marchetti, M Martinelli, and R Simili, “The insb auger recombination coefficient derived from the ir-fir dynamical plasma reflectivity,” *Journal of Physics: Condensed Matter* **13**, 7363 (2001).
- [39] M. Oszwaldowski and M. Zimpel, “Temperature dependence of intrinsic carrier concentration and density of states effective mass of heavy holes in InSb,” *Journal of Physics and Chemistry of Solids* **49**, 1179 – 1185 (1988).
- [40] William P. Dumke, “Quantum theory of free carrier absorption,” *Phys. Rev.* **124**, 1813–1817 (1961).
- [41] Chihiro Hamaguchi, *Basic Semiconductor Physics (2nd edition)* (Springer, 2010).